Coastal Engineering 65 (2012) 19–26

Contents lists available at SciVerse ScienceDirect

Coastal Engineering

journal homepage: www.elsevier.com/locate/coastaleng

Bottom friction and wind drag for wave models

M. Zijlema *, G.Ph. van Vledder, L.H. Holthuijsen

Faculty of Civil Engineering and Geosciences, Delft University of Technology, Stevinweg 1, 2628CN, Delft, The Netherlands

ARTICLE INFO

Article history:
Received 4 January 2012
Received in revised form 29 February 2012
Accepted 2 March 2012
Available online 1 April 2012

Keywords:
Wave modelling
Bottom friction
Wind drag
SWAN
Texel storm
JONSWAP

ABSTRACT

Waves propagating in shallow water dissipate energy in a thin, turbulent boundary layer near the bottom. This friction can be estimated with a simple quadratic friction law scaled with an empirical coefficient. Two values of this coefficient have been recommended by previous studies (for sandy bottoms): a high value for waves in a storm and a low value for swell. We show here that, in contrast to current practise, the lower value should be used for both applications. The reason is that the high value, dating from the early 1980s, was inferred from observations in a severe storm using a relatively high wind drag. Our review of a large number of more recent observations, gives a new wind drag parameterization with lower values. With this new parameterization we infer from the same storm the lower value of the bottom friction coefficient. Using this lower value also improves the estimates of wave growth in shallow water and of low-frequency wave decay in a tidal inlet, independent of the wind drag.

1. Introduction

Waves propagating in shallow water dissipate energy in a thin, turbulent boundary layer near the bottom ($kd \leq 3$, say, where k is wave number and d is depth). The modelling of this dissipation varies from rather simple to quite complex, but always involving some empirical coefficient(s). Excellent reviews have been given by the WISE group (2007) and others (e.g., Luo and Monbaliu, 1994). A relatively simple but successful model has been suggested by JONSWAP (Hasselmann et al., 1973) with a constant bottom friction coefficient χ. JONSWAP suggested using a value $\chi = 0.038\ m^2s^{-3}$ for swell dissipation over sandy bottoms. Later, Bouws and Komen (1983) suggested for the same model but for fully developed wind-seas a higher value $\chi = 0.067\ m^2s^{-3}$. We have reasons to re-examine these values, in particular whether or not preference should be given to the lower JONSWAP value. This is relevant for presently operational wave prediction models which use this approach (e.g., the WAM model, WAMDI, 1988; the SWAN model, Booij et al., 1999; the Wavewatch III® model, Tolman and Chalikov, 1996; Tolman, 2009; the WWMII model Roland et al., 2009; the MIKE21 OSW3G model; Johnson and Kofoed-Hansen, 2000; the STWAVE model, Smith, 2007).

Hindcasts of waves in shallow water show that the high value of χ tends to over-estimate the wave dissipation (Brown, 2010; Groeneweg et al., 2008; Padilla-Hernández and Monbaliu, 2001; Van Vledder et al., 2008). This high value was estimated from observations in a storm which requires estimates of wind and white capping effects. Recent observations of the wind drag coefficient C_d at high wind speeds suggest that the wind effect was over-estimated in that storm. The low value $\chi = 0.038\ m^2s^{-3}$ seems to be the more accurately as it was obtained from swell observations, which do not require wind estimates.

This paper is organised as follows. In Section 2, we briefly describe the bottom friction formulation and the background of estimating the two values of the bottom friction coefficient. In Section 3 we introduce an alternative parameterization of the *wind* drag coefficient which affects the estimation of the *bottom* friction coefficient. In Section 4 we show the effect of using the low bottom friction on wave growth in shallow water and on the penetration of low-frequency energy through a tidal inlet under storm conditions. We conclude our presentation in Section 5 with a summary and conclusions.

2. Estimates of the bottom friction

Hasselmann et al. (1973) observed swell in shallow water during the Joint North Sea Wave Project (JONSWAP) and estimated the bottom friction coefficient directly from the observed decay. Bouws and Komen (1983) estimated the same coefficient in a severe storm by closing the local energy balance of the waves. Both approaches are briefly described here.

2.1. JONSWAP

During JONSWAP, Hasselmann et al. (1973) observed several hundred spectra in shallow water with well-defined low-frequency swell peaks. As these were tracked along a number of observation stations,

* Corresponding author. Tel.: +31 15 783255; fax: +31 15 2784842.
E-mail addresses: m.zijlema@tudelft.nl (M. Zijlema), g.p.vanvledder@tudelft.nl (G.P. van Vledder), l.h.holthuijsen@tudelft.nl (L.H. Holthuijsen).

0378-3839/$ – see front matter
doi:10.1016/j.coastaleng.2012.03.002

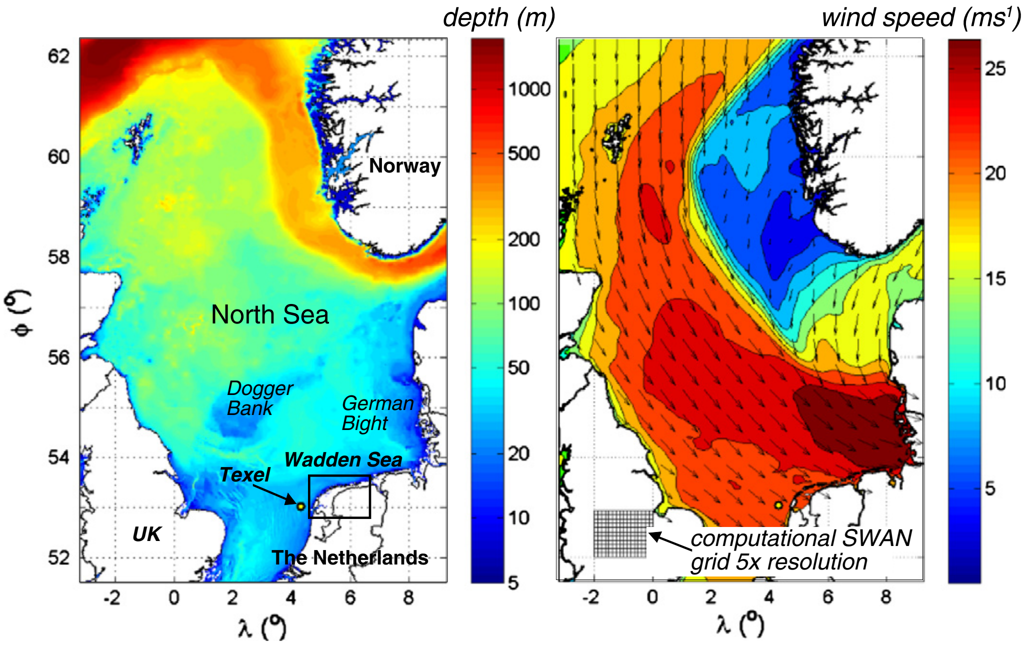

Fig. 1. Left-hand panel: the bathymetry in the North Sea, the location of the observations (Texel) and the location of the Wadden Sea. Right-hand panel: the wind field for the Texel storm (Jan. 3rd, 1976, 12:00 GMT) from the HIRLAM atmospheric model. Area shown is the computational area for SWAN with part of the computational grid (actual grid resolution is 5× finer than shown).

the dissipation of these swells could be quantified. The corresponding bottom friction coefficient was estimated on the basis of a quadratic friction law for the bottom shear stress:

$$\tau_b = \rho_w C_b u_b^2 \tag{1}$$

in which τ_b is the shear stress, ρ_w is the density of water, C_b is a bottom drag coefficient and u_b is the current velocity just outside the turbulent bottom boundary layer. For spectral wave models, its effect is formulated in terms a source term in the energy balance of short-crested, random waves with an energy density spectrum varying in time and space $E(f, \theta, x, y, t)$:

$$\begin{aligned}&\frac{\partial E(f,\theta;x,y,t)}{\partial t}+\frac{\partial c_{g,x}E(f,\theta;x,y,t)}{\partial x}+\frac{\partial c_{g,y}E(f,\theta;x,y,t)}{\partial y}\\&\quad+\frac{\partial c_\theta E(f,\theta;x,y,t)}{\partial\theta}\\&\quad=S(f,\theta;x,y,t)\end{aligned} \tag{2}$$

The first term in the left-hand side represents the local rate of change of energy density in time, the second and third terms represent propagation in geographical space (with propagation velocities $c_{g,\,x}$ and $c_{g,\,y}$ in x- and y-space, respectively, thus accounting for shoaling in limited depth). The fourth term represents refraction (with propagation velocity c_θ in θ-space). The term $S(\sigma, \theta)$ is the source term representing wave generation by wind, nonlinear wave-wave interactions and dissipation. Using linear wave theory, Hasselmann et al. (1973) formulate the source term for bottom friction $S_b(f, \theta)$ based on Eq. (1) as

$$S_b(f,\theta) = -\chi\frac{\rho g k^2 E(f,\theta)}{(2\pi f)^2\cosh^2 kd} \tag{3}$$

in which f is frequency, θ is direction, k is wave number, d is depth, the bottom friction coefficient $\chi = C_b g u_{rms,\,b}$ in which $u_{rms,\,b}$ is the root-mean-square orbital velocity near the bottom. In general bottom dissipation depends on the bottom material and related parameters such as grain diameter in the case of sand and also bed shapes such as ripples, or wave induced bed movement. However, properly representing the effects of these variations requires detailed information which is often not available. By default therefore, the engineer is often forced to revert to a simple approach such as the JONSWAP approach with a fixed value of χ. JONSWAP used 678 spectra from 10 cases to estimate this value from the observed swell decay. The values per case thus found varied from $\chi = 0.0019\ m^2s^{-3}$ to $\chi = 0.160\ m^2s^{-3}$ with an average of 0.038 m^2s^{-3} (weighted with the number of spectra per case) and a standard deviation of 0.042 m^2s^{-3} (from Table 3 in Hasselmann et al., 1973).

2.2. The Texel storm

Bouws and Komen (1983) obtained estimates of χ for locally generated waves by analysing the energy balance of the waves at a fixed location during a severe storm in the southern North Sea (the Texel storm). The location of the observations was 25 km west of the island of Texel (Fig. 1) where the water depth is approximately 30 m. The bottom material in the up-wind area where the waves were generated varies from fine sand to gravel.

The maximum wind speed at the location of the observations was ~26.5 m/s but it was ~30 m/s in the German Bight (to the North-East). The observed significant wave height[1] H_{m0} at the Texel location increased from ~5 m to ~7 m during the first 6 h of the storm but then remained fairly constant for 15 h (between 6:00 GMT and 21:00 GMT; Fig. 2). The mean wave period $T_{m0,\,1} = m_0/m_1$ correspondingly increased from ~7 s to ~10 s.

This stationary character of the wind and the waves motivated Bouws and Komen (1983) to remove time as a variable in their analysis. They averaged the observed spectra and estimated for this average spectrum the source terms for wind input, quadruplet wave–wave interactions and white capping. Bottom induced breaking was ignored and tidal effects were deemed to be negligible. The effect of

[1] Estimated from the observed spectra as $H_{m0} = 4\sqrt{m_0}$, where $m_n = \int_0^\infty f^n E^*(f)df$ is the n^{th}-order moment of the variance density spectrum $E^*(f) = \int E(f,\theta)/(\rho g)d\theta$.

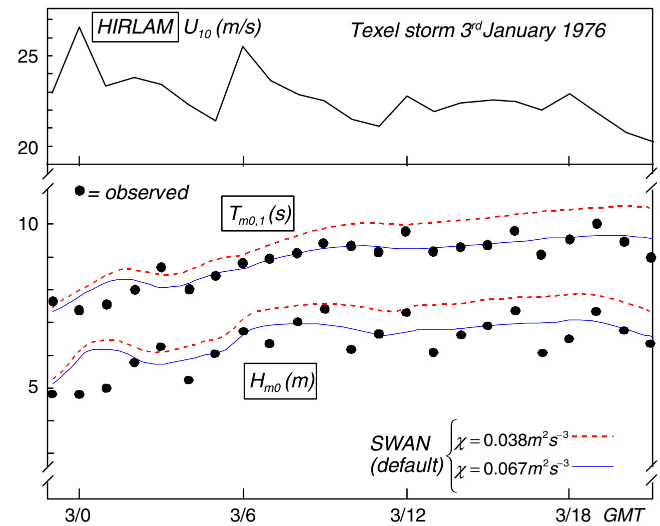

Fig. 2. Upper panel: the wind speed during the Texel storm as computed with the HIRLAM atmospheric model as a function of time at the location of wave observations. Lower panel: the significant wave height (lower data points) and mean wave period (upper data points) at the Texel location as observed and as computed with the SWAN wave model with default wind drag and high and low bottom friction.

propagation was estimated with a scaling of the spectrum that later became known as the TMA scaling (Bouws et al., 1985). They estimated the coefficient χ and the scaling coefficient η for white capping by closing the energy balance (using $U_{10} = 25$ m/s wind speed). They thus found $\chi = 0.067\ m^2 s^{-3}$ and $\eta = 1.9x10^{-4}\ s$.

Later, Weber (1991) used a spectral wave model to hindcast the waves in the same storm. In contrast to the approach of Bouws and Komen (1983), this model accounts explicitly for the spatial variability of wind, waves and depth. The model was identical to the WAM model (WAMDI, 1988), except that refraction was not considered. With the low value for the bottom friction coefficient $\chi = 0.038\ m^2 s^{-3}$, this hindcast over-predicted the significant wave height at the Texel location by ~1 m. This result supports the result of Bouws and Komen (1983) in the sense that a higher C_b value would be required to obtain agreement with the observed wave conditions. Further south, Weber (1991) considers the waves to be swell. Here the hindcast results agreed with the observations. This suggests that $\chi = 0.038\ m^2 s^{-3}$ is a proper value to use for swell, in agreement with the findings of JONSWAP.

We repeated the hindcast of this storm with the SWAN wave model (Booij et al., 1999) in default mode. This model is also identical to the WAM model (WAMDI, 1988) but only in the sense that the same propagation formulations and the same source terms are used, except that (a) a linear wind growth term has been added (to initialize the wave field; Cavaleri and Malanotte-Rizzoli, 1981; Tolman, 1992) and (b) we shifted the dissipation due to white capping to higher frequencies (Rogers et al., 2003). In both models, the formulation of wind input is due to Snyder et al. (1981) and Komen et al. (1984), for the quadruplet wave-wave interactions it is due in deep water to Hasselmann et al. (1985) and in finite-depth water to the Komen et al. (1994, p. 228) approximation of Hasselmann and Hasselmann (1981). For white capping it is due to Komen et al. (1984). In *shallow* water, SWAN additionally accounts for depth-induced breaking and triad wave-wave interactions (both found to be irrelevant for the present study). Otherwise the models differ only in their numerical techniques. The wind field was based on a re-analysis by blending a high resolution local area model (HIRLAM; e.g., Cats and Wolters, 1996) in the large-scale wind fields of the ECMWF archive (European Centre for Medium-Range Weather Forecasts). The wind speeds at the Texel location thus obtained is ~10% lower than those estimated by Bouws and Komen (1983) and Weber (1991). We are not aware of observations that could be used to verify these estimates. The wind field was given with a time step of 1 h. The wave computations were carried out with a 10 min time step. The spatial resolution was $\Delta\lambda = 0.025^0$ (longitude) and $\Delta\varphi = 0.0167^0$ (latitude) for both the wind field and the wave field. Like Bouws and Komen (1983) and Weber (1991), we ignore bottom induced breaking and tidal effects but unlike these authors, we include refraction. The spatial resolution in our wave computations ~1.8 km is considerably finer than 75 km as in the hindcast of Weber (1991). The results for using either $\chi = 0.038\ m^2 s^{-3}$ or $\chi = 0.067\ m^2 s^{-3}$ in our hindcast are shown in Fig. 2. It is obvious that the high value of the friction coefficient is needed to obtain good agreement with the observations.

These hindcast results of both Weber (1991) and the present study are consistent with the χ values suggested by JONSWAP and Bouws and Komen (1983) in the sense that $\chi > 0.038\ m^2 s^{-3}$ is needed in the storm and that $\chi = 0.038\ m^2 s^{-3}$ is adequate for swell. However, we have two reasons to re-assess this finding. First, recent observations of the wind drag suggest considerably lower energy input to the waves by the wind and second, SWAN consistently under-estimates low-frequency energy in tidal inlets and estuaries when using $\chi = 0.067\ m^2 s^{-3}$ (Brown, 2010; Groeneweg et al., 2008; Van Vledder et al., 2008). In addition, Padilla-Hernández and Monbaliu (2001) find better results predicting the significant wave height and peak period of the waves in the shallow water Lake George (Australia) when using $\chi = 0.038\ m^2 s^{-3}$.

3. Wind drag and bottom friction

The parameterization of the *wind* drag coefficient which is used in SWAN dates from 1982 and gives fairly high values compared to more recent observations, particularly at high wind speeds. Here, we propose a new parameterization and show that it is consistent with the wave observations in the Texel storm if the low bottom friction coefficient is used.

3.1. Wind drag coefficient

The source term for energy input by wind in SWAN is driven by the friction wind velocity u_*. Since the wind fields are formulated in terms of the wind speed at 10 m elevation, U_{10}, SWAN requires a transformation from U_{10} to u_*. This transformation is carried out with the conventional expression $u_*^2 = C_D U_{10}^2$. The value of the wind drag coefficient C_D in SWAN is due to Wu (1982), supplemented with an imposed lower limit (WAMDI, 1988):

$$C_D = \begin{cases} 1.2875x10^{-3} & \text{for } U_{10} < 7.5\,\text{m/s} \\ (0.8 + 0.065\ U_{10})x10^{-3} & \text{for } U_{10} \geq 7.5\ \text{m/s} \end{cases} \tag{4}$$

Recent observations indicate that this and similar parameterization (e.g., Garratt, 1977) over-estimates the drag coefficient at high wind speeds ($U_{10} > 20$ m/s, say). This is sometimes remedied in operational wave and storm surge prediction models by capping the C_D value at a limiting value (e.g., ~2.5×10^{-3} in the CSOWM wave model, Khandekar et al., 1994 and ~3.5×10^{-3} in the ADCIRC storm surge and circulation model, Dietrich et al., 2011). In Fig. 3 we show the C_D values from nine authoritative studies. Smith and Banke (1975; their Fig. 3) includes 3 data sets. We averaged these data over 2 m/s wind speed bins. The study of Garratt (1977; his Fig. 3) includes 14 data sets which we averaged over 2 m/s wind speed bins. Large and Pond (1981; their Fig. 6) give average values in 1.5–3 m/s wind speed bands. Wu (1982) reviews 8 data sets from which we removed the two hurricanes analysed by Miller (1964) as these were affected by land. Powell et al. (2003) give values based on observed wind profiles in 4 layers (differing in height and thickness) in the

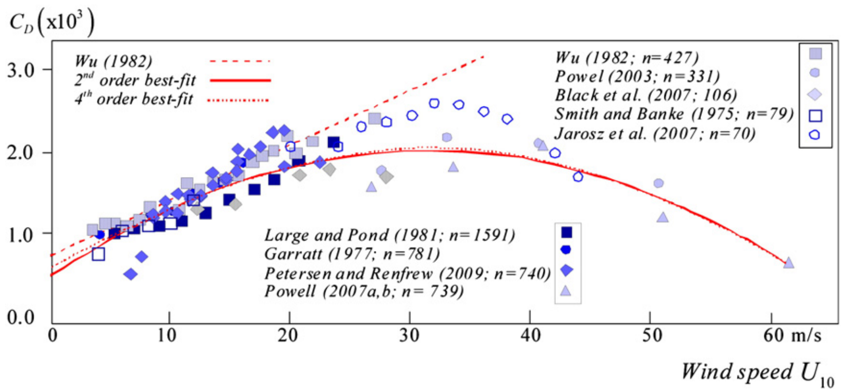

Fig. 3. Observed values of the wind drag coefficient C_d from various studies and the weighted best-fit 2nd- and 4th-order polynomial (n is the number of independent data points per study).

atmospheric boundary layer for four different wind speeds $27.5<U_{10}<50.5$ *m/s*. We averaged the values over the four layers. This study included 6 other data sets. Black et al. (2007; their Fig. 5) give average values at five wind speeds $12<U_{10}<28$ *m/s*. We averaged the observations of Jarosz et al. (2007) over 2 m/s wind speed bins. This study includes 1 other data set. Powell (2007a,b) gives average values from 2 layers in the atmospheric boundary layer at five different wind speeds $26.8<U_{10}<61.5$ *m/s*. We use the average from the 20–160 m layer (at the advice of M.D. Powell, personal communication, 2011). Petersen and Renfrew (2009; their Fig. 8) give median value in 1 m/s wind speed bins with at least 10 data points in each bin. This study includes 4 other data sets. To avoid including data sets twice or more in our averaging, we removed any overlap between these nine studies. If an older study A and a younger study B shared the same data set Q, then data set Q was removed from the younger study B. In this way any data set Q is considered only once. Occasionally a data set Q could not be removed because it was already included in averages of a study that included other data sets.

These observations show convincingly (Fig. 3) that C_D increases almost linearly with wind speed up to ~20 m/s, then levels off and decreases again at ~35 m/s to rather low values at 60 m/s wind speed. This is quite different from the behaviour suggested by the parameterization of Wu (1982), which is an unbounded linear function of wind speed with (considerably) higher values for wind speeds over 20 m/s. The levelling off and decrease at high wind speeds is qualitatively supported by other field data (Amorocho and DeVries, 1980; Wu, 1969), by laboratory observations (Donelan et al., 2004) and by an inverse modelling of the wave hindcast in a hurricane (Yokota et al., 2010). There is also theoretical support for such behaviour at high wind speeds (Bye and Jenkins, 2006; Bye and Wolff, 2008; Kudryavtsev, 2006; Kudryavtsev and Makin, 2007; Makin, 2005; Soloviev and Lukas, 2010). However, it must be noted that the energy transfer to the waves estimated from such airside observations seems to under-estimate the observed wave growth (e.g., Belcher and Hunt, 1998; Peirson and Garcia, 2008). That would invalidate the scaling of wave growth with a C_D-based friction velocity. But, the above observations of Jarosz et al. (2007; Fig. 3) do not show such discrepancy. These observations were derived from the momentum balance in the upper ocean under a hurricane and show behaviour consistent with the airside observations, certainly at very high wind speeds. These aspects are important and need to be resolved but we consider this beyond the scope of the present study.

We fitted a 2nd and a 4th-order polynomial to the data of Fig. 3, using the number of independent observations in each data set as a weight. This puts more emphasis on the solid black symbols than on the grey or blank symbols in Fig. 3, and explains the preference for the low observed C_D values. The differences between the two best-fit polynomials are barely noticeable and then only for very low wind speeds (<5 m/s). We therefore adopted the simplest, i.e., the 2nd order polynomial:

$$C_D = \left(0.55 + 2.97\ \tilde{U} - 1.49\ \tilde{U}^2\right) x\, 10^{-3} \tag{5}$$

in which $\tilde{U} = U_{10}/U_{ref}$ and the reference wind $U_{ref} = 31.5$ *m/s* is the wind speed at which C_D attains its maximum value in this expression. These C_d values are lower than in the expression of Wu (1982) by 10%–30% for high wind speeds ($15 \leq U_{10} \leq 32.6$ *m/s*) and over 30% for hurricane wind speeds ($U_{10} \geq 32.6$ *m/s*).

3.2. The Texel storm

We repeated the hindcast of the Texel storm with the 2nd order polynomial estimate of C_D. The results are given in Fig. 4. It is remarkable that with the low bottom friction the results are close to the results obtained with high bottom friction in Fig. 2. The differences are only noticeable in slightly higher mean wave periods in the tail of the storm. We conclude from this that the energy balance of the waves is consistent with the observations if (a) the default wind drag (Eq. (3)) is combined with high bottom friction $\chi = 0.067\ m^2 s^{-3}$ or (b) the new wind drag (Eq. (4)) is combined with $\chi = 0.038\ m^2 s^{-3}$. No preference of one over the other combination can be based on these results. But in view of the larger data base of the new wind drag parameterization, the second combination seems preferable.

4. Wave growth and decay

Before coming to a final conclusion, we consider the effect of using the low value of χ on wave generation in shallow water and low-frequency wave decay in a tidal inlet.

4.1. Shallow water wave growth

We consider waves generated by a constant wind blowing perpendicularly off a long and straight coast line over water with a constant depth. Possibly the best sets of observations in such a situation are due to Young and Verhagen (1996) and Young and Babanin (2006) who obtained their observations in Lake George (Australia). The bottom material of this lake is fine clay (personal communication L.A. Verhagen, 1996). They presented the dimensionless wave energy $\tilde{E} = g^2 E_{tot}/U_{10}^4$ (where $E_{tot} = m_0$) as a function of dimensionless fetch $\tilde{F} = gF/U_{10}^2$ (where F is the fetch or the distance to the up-wind coast), and dimensionless depth $\tilde{d} = gd/U_{10}^2$ (where d is the depth). To emphasize the depth-limited results, we consider only the fully

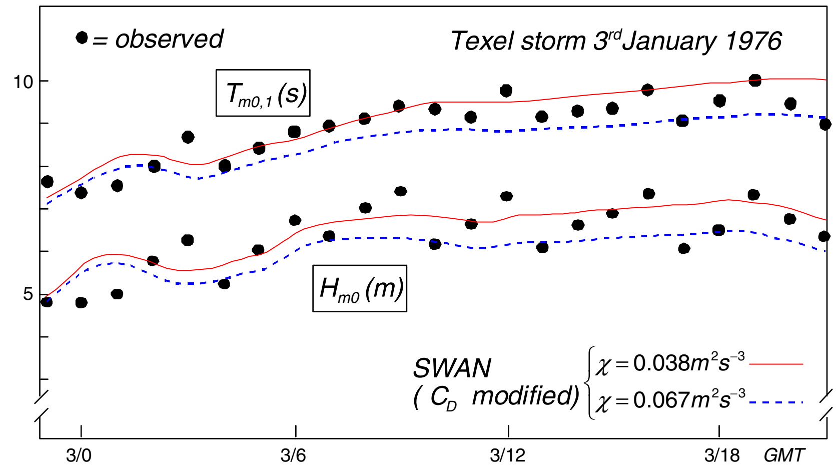

Fig. 4. The significant wave height (lower data points) and mean wave period (upper data points) at the Texel location as observed and as computed with the SWAN wave model with the new wind drag and high and low bottom friction.

developed situation so that the dimensionless wave energy is a function of dimensionless depth only. In addition, we consider only those cases in which bottom friction dominates depth-induced breaking and white capping. We verified this by inter-comparing the integrated source terms for these cases as computed with SWAN over the range of dimensionless depth $0.01 < \tilde{d} < 1$. Although Young and Verhagen (1996) and Young and Babanin (2006) presented their results in dimensionless form, we used for our final computations the actually observed value of depth and wind speed U_{10}. This limited the cases to 10 cases of Young and Babanin (2006; Young and Verhagen, 1996 do not provide the actual depth and wind speed). The results of our computations are given in dimensionless form in Fig. 5, which shows again that for $\chi = 0.038\ m^2s^{-3}$ the results agree very well with the observations (located slightly below the envelope of Young and Babanin, 2006) and much better than for $\chi = 0.067\ m^2s^{-3}$. This result is remarkable in the sense that the bottom material in Lake George is fine clay rather than sand for which the JONSWAP bottom friction coefficient $\chi = 0.038\ m^2s^{-3}$ would nominally be valid (coming from the southern North Sea). We verified that these results were insensitive to using the drag law of Wu (1982) or the new parameterization of Eq. (5).

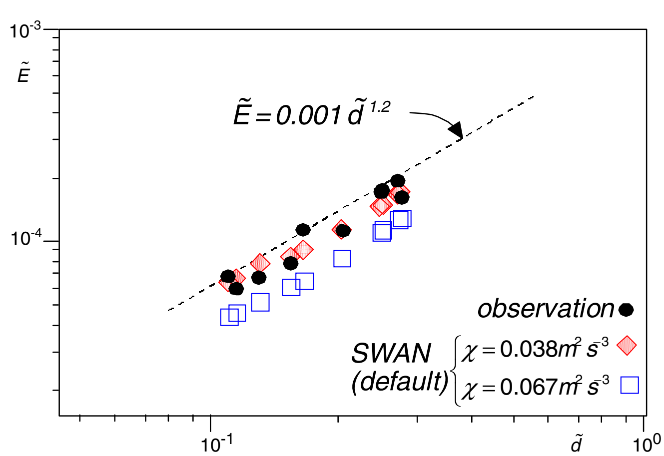

Fig. 5. Observations and parameterization of Young and Babanin (2006) of dimensionless wave energy for fully developed waves in shallow water as a function of dimensionless depth (over the depth range with bottom friction dominance) and the computational SWAN results with high and low bottom friction.

4.2. Low-frequency decay

Groeneweg et al. (2008) and Van Vledder et al. (2008) observed in their hindcast studies of storms in the Wadden Sea (in the southern North Sea; Fig. 1) that the decay of low-frequency wave energy over the tidal flats is significantly over-estimated by SWAN in default mode. Zijlema (2008) showed that this may be due to over-estimating the bottom friction when using $\chi = 0.067\ m^2s^{-3}$. To further investigate this, we repeated a number of these hindcasts with emphasis on the Amelander Zeegat where the phenomenon was most noticeable. This is the tidal inlet between the islands of Ameland and Terschelling with a 25 m deep channel penetrating deep into the Wadden Sea. The area is protected from the open sea by an outer tidal delta with a minimum depth of ~7 m during the cases considered here.

The wave conditions were observed during three severe westerly storms with two arrays of 6 wave buoys each, but we verified that the waves were sensitive to the value of the friction coefficient χ at only 4 buoys — at the other buoys, low-frequency energy (below 0.15 Hz) was absent. These 4 buoys (AZB21, AZB22, AZB31 and AZB32; Fig. 6) were located in the tidal inlet just inland from the ebb tidal delta. A total of 3 representative cases were chosen around the peak of these storms: January 11th at 13 h00, January 18th at 14 h00 and March 18th at 10 h00 (local time = GMT + 1). These cases are characterized by high wind speeds ($U_{10} = 20$ m/s on average). The wind directions of these cases remained in the 230°–280° directional sector (Nautical convention). For each of the cases, water level and current fields were computed with a circulation model that includes tidal, wind and wave forcing (Groeneweg et al., 2008). Up-wind wave information is taken from two deep water directional buoys west of the area (ELD and SON; Fig. 6; we verified with computations on a larger scale that these boundary conditions barely changed from east to west). To accommodate the high geographic variability of the bathymetry we used an unstructured grid for both the bathymetry and the computations (Zijlema, 2008) with the highest resolution of 10 m near the 4 buoys. The travel time of the waves through the model area is small compared to the time scale of atmospheric and hydrodynamic variations, so that the simulations were carried out in stationary mode. We show 4 of the most illustrative spectra in Fig. 7. On the basis of the computed spectra we choose $f = 0.15\ Hz$ as the upper limit of the low-frequency band. It is obvious from these results that the levels of energy density in this band agree better with the observations when using the low bottom friction rather than the high bottom friction. The choice between high and low bottom friction has little or no effect at *higher* frequencies. The

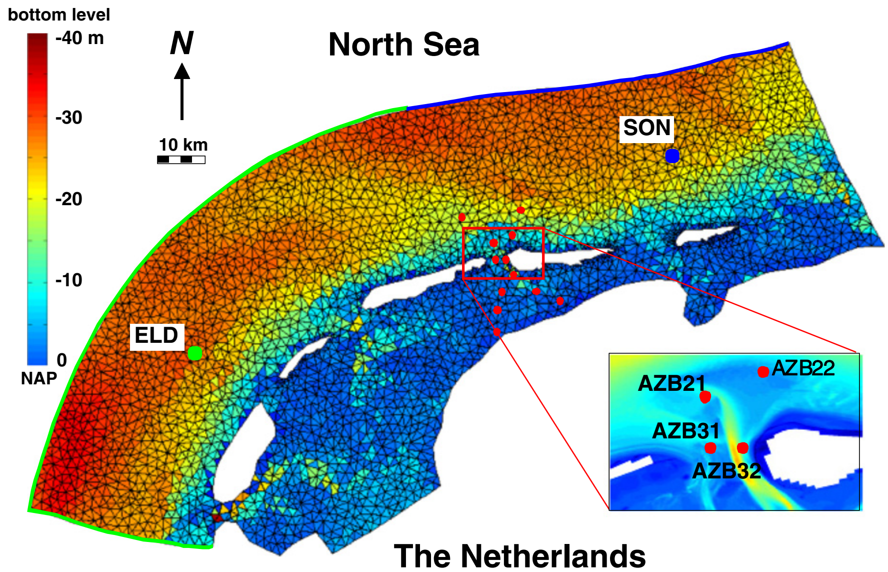

Fig. 6. Bathymetry of the Wadden Sea, buoy locations (bottom level in m relative to Amsterdam Ordnance Datum or NAP) and unstructured computational grid (fine resolution not shown). Wave conditions of buoys ELD (green dot) and SON (blue dot) imposed along boundaries of the same colour as the buoy locations.

comparison between observed and computed low-frequency significant wave height $H_{0.15}$ (defined here as $H_{0.15}=4\sqrt{m_{0.15}}$ where $m_{0.15}$ is the integral of the spectrum over the low-frequency band) is given in Fig. 8. It is obvious that the results for the low-frequency energy are slightly better using $\chi=0.038\ m^2s^{-3}$ than using $\chi=0.067\ m^2s^{-3}$ even if there is still a considerable underestimation of the high-energy observations possibly due to overestimating the dissipation by depth-induced breaking. The scatter index for $H_{0.15}$, defined as the rms-error normalized with the mean of the observed values, is reduced from $s.i.=0.27$ to $s.i.=0.19$ when the lower bottom friction is used. The corresponding bias is reduced from $\Delta=-0.30\,m$ to $\Delta=-0.19\,m$ (under-prediction). The results would improve further without bottom friction. In fact, we found that the scatter index would reduce to $s.i.=0.11$ and the bias to $\Delta=-0.05\,m$. This is a considerable improvement. However, there are four reasons against assuming such zero bottom friction. First, it is physically unrealistic. Second, the reduction in bias is due to an unrealistic increase in low-frequency energy compared to the

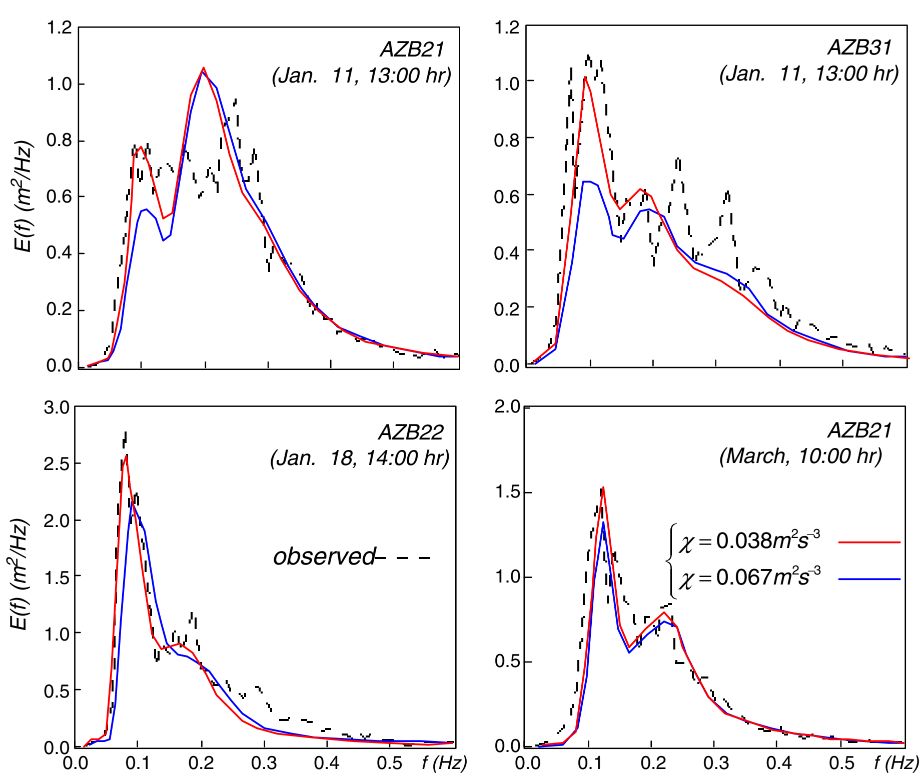

Fig. 7. Observed and computed spectra in the Wadden Sea at locations AZB21, AZB22 and AZB32 in the storms of Jan. 11th and 18th, 2007 and March 18th, 2007 for the high and the low bottom friction coefficient using default wind drag.

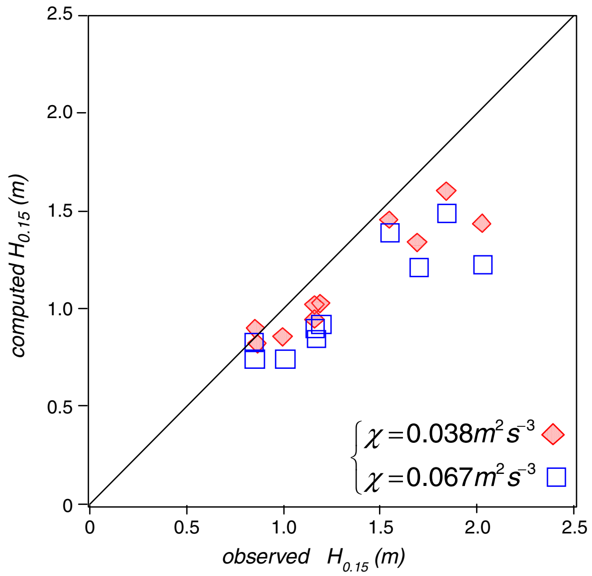

Fig. 8. Scatter plot of computed and observed low-frequency significant wave height $H_{0.15}$ at locations AZB21, AZB22, AZB31 and AZB32 with high and low bottom friction (as in Fig. 7). Not all buoys were operating in all cases.

observations (the bottom friction affects the higher frequencies only marginally). Third, the wave growth in Lake George would be unrealistically high. Fourth, we found that reducing depth-induced breaking (increasing the ratio of maximum wave height over depth ratio from the default value in SWAN $\gamma = 0.73$ to $\gamma = 0.8$) gives virtually the same improvement as a frictionless bottom, without the objections just mentioned and without affecting the results of the other computations of this study.

5. Summary and conclusions

In this study our concern was primarily with the scaling of the JONSWAP formulation of bottom friction for spectral wave models (Hasselmann et al., 1973) which use the source terms of the WAM model (WAMDI, 1988). During our analysis we formulated a new parameterization for the wind drag coefficient as a function of wind speed on the basis of a large number of observations from authoritative studies.

In default mode, the SWAN wave model uses the bottom friction coefficient $\chi = 0.067\ m^2 s^{-3}$ as recommended by Bouws and Komen (1983) for waves in storms. This recommendation is based on their analysis of observations in an extreme storm in the southern North Sea near the island of Texel. It is supported by the analysis of the same storm by Weber (1991) and by the present study when using a relatively high wind drag. However, we found that using both lower wind drag and lower bottom friction, provides essentially the same hindcast results in this storm. This motivated us to review a large number of published observations of the wind drag coefficient. Based on this, we propose a parameterization of the wind drag coefficient with considerably lower values at high wind speeds than the parameterization of Wu (1982) which is used in SWAN. This lower wind drag may seriously affect estimating waves and storm surges under design conditions for off-shore and coastal structures for which often $U_{10} > 30\ m/s$. Using this new wind drag parameterization requires using the low value of $\chi = 0.038\ m^2 s^{-3}$.

This lower value of the bottom friction coefficient also improves the agreement between the SWAN results and (generalized) observations of fully developed waves in shallow water in Lake George. This finding does not depend on the proposed wind drag which is virtually identical to the wind drag of Wu (1982) at the rather low wind speeds during these lake observations. The lower value of the bottom friction also improves the agreement between SWAN results and the observed penetration of low-frequency energy through the Amelander Zeegat under storm conditions. This finding too does not depend on the proposed wind drag as the distances involved are too short for the wind to have any significant effect.

Our final conclusions are therefore first, that the low value of the bottom friction coefficient $\chi = 0.038\ m^2 s^{-3}$ due to JONSWAP (Hasselmann et al., 1973) should be preferred for both swell and locally generated waves, at least for bottoms such as often found in shelf seas, tidal regions and lakes, with sand, possibly mixed with gravel and perhaps silt and fine clay but not for movable or porous bottoms (e.g., mud or a thick layer of gravel). Secondly, we find that our suggested parameterization of the wind drag given by Eq. (5) fits a large number of wind drag observations much better than the parameterization due to Wu (1982), particularly at high wind speeds, even if the later would be capped at $\sim 3 \times 10^{-3}$ as in some operational wave and storm surge prediction models.

Acknowledgements

We gratefully acknowledge the assistance of Jacco Groeneweg for providing us with the Wadden Sea data from the SWIVT data base of Deltares. We thank Frank Lantsheer of the Royal Netherlands Meteorological Institute (KNMI) for providing us with the wind field of the Texel storm.

References

Amorocho, J., DeVries, J.J., 1980. A new evaluation of the wind stress coefficient over water surfaces. Journal of Geophysical Research 85 (C1), 433–442.
Belcher, S.E., Hunt, J.C.R., 1998. Turbulent flow over hills and waves. Annual Review of Fluid Mechanics 30, 507–538.
Black, P.G., D'Asaro, E.A., Drennan, W.M., French, J.R., Niiler, P.P., Sanford, T.B., Terrill, E.J., Walsh, E.J., Zhang, J.A., 2007. Air-sea exchange in hurricanes: synthesis of observations from the coupled boundary layer air–sea transfer experiment. Bulletin of the American Meteorological Society 88 (3), 357–374.
Booij, N., Ris, R.C., Holthuijsen, L.H., 1999. A third-generation wave model for coastal regions, Part I, model description and validation. Journal of Geophysical Research 104 (C4), 7649–7666.
Bouws, E., Komen, G.J., 1983. On the balance between growth and dissipation in an extreme, depth-limited wind–sea in the southern North Sea. Journal of Physical Oceanography 13 (9), 1653–1658.
Bouws, E., Günther, H., Rosenthal, W., Vincent, C.L., 1985. Similarity of the wind wave spectrum in finite depth water. 1. Spectral form. Journal of Geophysical Research 90 (C1), 975–986.
Brown, J.M., 2010. A case study of combined wave and water levels under storm conditions using WAM and SWAN in a shallow water application. Ocean Modelling 35, 215–229.
Bye, J.A.T., Jenkins, A.D., 2006. Drag coefficient reduction at very high wind speeds. Journal of Geophysical Research 111 (C03024). doi:10.1029/2005JC003114.
Bye, J.A.T., Wolff, J.-O., 2008. Charnock dynamics: a model for the velocity structure in the wave boundary layer of the air–sea interface. Ocean Dynamics 58, 31–42.
Cats, G., Wolters, L., 1996. The HIRLAM project. IEEE Computational & Engineering 3 (4), 4–7.
Cavaleri, L., Malanotte-Rizzoli, P., 1981. Wind wave prediction in shallow water: theory and applications. Journal of Geophysical Research 86 (Cll), 10, 961–10, 973.
Dietrich, J.C., Zijlema, M., Westerink, J.J., Holthuijsen, L.H., Dawson, C., Luettich, R.A., Jensen, R.E., Smith, J.M., Stelling, G.S., Stone, G.W., 2011. Modeling hurricane waves and storm surge using integrally-coupled scalable computations. Coastal Engineering 58, 45–65.
Donelan, M.A., Haus, B.K., Reul, N., Plant, W.J., Stiassnie, M., Graber, H.C., Brown, O.B., Saltzman, E.S., 2004. On the limiting aerodynamic roughness of the ocean in very strong winds. Geophysical Research Letters 31, L18306.
Garratt, J.R., 1977. Review of drag coefficients over oceans and continents. Monthly Weather Review 105, 915–929.
Groeneweg, J., van der Westhuysen, A.J., van Vledder, G.Ph., Jacobse, S., Lansen, J., van Dongeren, A.R., 2008. Wave Modelling in a tidal inlet: performance of SWAN in the Wadden Sea. 31st Int. Conf. Coastal Eng. ASCE, pp. 411–423.
Hasselmann, S., Hasselmann, K., 1981. A symmetrical method of computing the nonlinear transfer in a gravity-wave spectrum. Hamb. Geophys. Einzelschriften. Reihe A: Wiss. Abhand., 52 (8). Geophys. Inst. Univ. of Hamburg, Hamburg, Germany. 138 pp.
Hasselmann, K., Barnett, T.P., Bouws, E., Carlson, H., Cartwright, D.E., Enke, K., Ewing, J.A., Gienapp, H., Hasselmann, D.E., Kruseman, P., Meerburg, A., Müller, P., Olbers, D.J., Richter, K., Sell, W., Walden, H., 1973. Measurements of wind-wave growth

and swell decay during the Joint North Sea Wave Project (JONSWAP). Deutsche Hydrographische Zeitschrift Suppl. A8 (12) 95 pp.
Hasselmann, S., Hasselmann, K., Allender, J.H., Barnett, T.P., 1985. Computations and parameterizations of the nonlinear energy transfer in a gravity wave spectrum, Part II, parameterizations of the nonlinear transfer for applications in wave models. Journal of Physical Oceanography 15 (11), 1378–1391.
Jarosz, E., Mitchell, D.A., Wang, D.W., Teague, W.J., 2007. Bottom-up determination of air–sea momentum exchange under a major tropical cyclone. Science 315, 1707–1709. doi:10.1126/science.1136466.
Johnson, H.K., Kofoed-Hansen, H., 2000. Influence of bottom friction on sea surface roughness and its impact on shallow water wind wave modeling. Journal of Physical Oceanography 30, 1743–1756.
Khandekar, M.L., Lalbeharry, R., Cardone, V., 1994. The performance of the Canadian spectral ocean wave model (CSOWM) during the Grand banks ERS-1 SAR wave spectra validation experiment. Atmosphere-Ocean 32 (1), 31–60.
Komen, G.J., Hasselmann, S., Hasselmann, K., 1984. On the existence of a fully developed wind–sea spectrum. Journal of Physical Oceanography 14 (8), 1271–1285.
Komen, G.J., Cavaleri, L., Donelan, M., Hasselmann, K., Hasselmann, S., Janssen, P.A.E.M., 1994. Dynamics and modelling of ocean waves. Cambridge University Press, Cambridge. 531 pp.
Kudryavtsev, V.N., 2006. On the effect of sea drops on the atmospheric boundary layer. Journal of Geophysical Research 111 (C07020). doi:10.1029/2005JC002970.
Kudryavtsev, V.N., Makin, V.K., 2007. Aerodynamic roughness of the sea surface at high winds. Boundary-Layer Meteorology 125, 289–303.
Large, W.G., Pond, S., 1981. Open ocean momentum flux measurements in moderate to strong winds. Journal of Physical Oceanography 11, 324–336.
Luo, W., Monbaliu, J., 1994. Effects of the bottom friction formulation on the energy-balance for gravity-waves in shallow-water. Journal of Geophysical Research 99 (C9), 18501–18511.
Makin, V.K., 2005. A note on the drag of the sea surface at hurricane winds. Boundary-layer Meteorology 115, 169–176.
Miller, B.I., 1964. A study of the filling of hurricane Donna (1960) over land. Monthly Weather Review 92 (9), 389–406.
Padilla-Hernández, R., Monbaliu, J., 2001. Energy balance of wind waves as a function of the bottom friction formulation. Coastal Engineering 43, 131–148.
Peirson, W.L., Garcia, A.W., 2008. On the wind-induced growth of slow water waves of finite steepness. Journal of Fluid Mechanics 608, 243–274.
Petersen, G.N., Renfrew, I.A., 2009. Aircraft-based observations of air–sea fluxes over Denmark Strait and the Irminger Sea during high wind speed conditions. The Quarterly Journal of the Royal Meteorological Society 135, 2030–2045.
Powell, M.D., 2007a. Drag coefficient distribution and wind speed dependence in tropical cyclones. Final Report to the National Oceanic and Atmospheric Administration (NOAA) Joint Hurricane Testbed (JHT) Program. 26 pp.
Powell, M.D., 2007b. New findings on Cd behavior in tropical cyclones. 28th Conference on Hurricanes and Tropical Meteorology paper 3D1.
Powell, M.D., Vickery, P.J., Reinhold, T.A., 2003. Reduced drag coefficient for high wind speeds in tropical cyclones. Nature 422, 279–283.
Rogers, W.E., Hwang, P.A., Wang, D.W., 2003. Investigation of wave growth and decay in the SWAN model: three regional-scale applications. Journal of Physical Oceanography 33 (2), 366–389.
Roland, A., Cucco, A., Ferrarin, C., Hsu, T.-W., Liau, J.-M., Ou, S.-H., Umgiesserand, G., Zanke, U., 2009. On the development and verification of a 2-D coupled wave-current model on unstructured meshes. Journal of Marine Systems 78, S244–S254.
Smith, J.A., 2007. Full-Plane STWAVE with bottom friction: II Model overview, US Army Corps of Engineers, Engineer Research and Development Center. Technical Report ERDC/CHL CHETN-1-75. 15 pp.
Smith, S.D., Banke, E.G., 1975. Variation of the sea surface drag coefficient with wind speed. Quarterly Journal Royal Meteorological Society 101, 665–673.
Snyder, R.L., Dobson, F.W., Elliott, J.A., Long, R.B., 1981. Array measurement of atmospheric pressure fluctuations above surface gravity waves. Journal of Fluid Mechanics 102, 1–59.
Soloviev, A., Lukas, R., 2010. Effects of bubbles and sea spray on air-sea exchange in hurricane conditions. Boundary-Layer Meteorology 136, 365–376. doi:10.1007/s10546-010-9505-0.
Tolman, H.L., 1992. Effects of numerics on the physics in a third-generation wind-wave model. Journal of Physical Oceanography 22, 1095–1111.
Tolman, H.L., 2009. User manual and system documentation of WAVEWATCH III™ version 3.14. Techn. Note 276, NOAA/NWS/NCEP/MMAB, 194 pp. + appendices. .
Tolman, H.L., Chalikov, 1996. Source terms in a third-generation wind wave model. Journal of Physical Oceanography 26, 2497–2518.
Van Vledder, G.Ph., Groeneweg, J., van der Westhuysen, A.J., 2008. Numerical and physical aspects of wave modelling in a tidal inlet. 31st Int. Conf. Coastal Eng. ASCE, pp. 424–436.
WAMDI group, 13 authors, 1988. The WAM model — a third generation ocean wave prediction model. Journal of Physical Oceanography 18 (12), 1775–1810.
Weber, N., 1991. Bottom friction for wind sea and swell in extreme depth-limited situations. Journal of Physical Oceanography 21, 149–172.
WISE group, 2007. Wave modelling — the state of the art. Progress in Oceanography 75, 603–674.
Wu, J., 1969. Wind stress and surface roughness at air–sea interface. Journal of Geophysical Research 74 (2), 444–455.
Wu, J., 1982. Wind-stress coefficients over sea surface from breeze to hurricane. Journal of Geophysical Research 87 (C12), 9704–9706.
Yokota, M., Hashimoto, N., Kawaguchi, K., Kawai, H., 2010. Development of an inverse estimation method of sea surface drag coefficient under strong wind conditions. 32nd Int. Conf. Coastal Eng. ASCE. Paper 32. 10 pp.
Young, I.R., Babanin, A.V., 2006. The form of the asymptotic depth-limited wind wave frequency spectrum. Journal of Geophysical Research 111 (C06031). doi:10.1029/2005JC003398.
Young, I.R., Verhagen, L.A., 1996. The growth of fetch limited waves in water of finite depth. Part 1. Total energy and peak frequency. Coastal Engineering 29, 47–78.
Zijlema, M., 2008. Parallel, unstructured mesh implementation for SWAN. 31st Int. Conf. Coastal Eng. ASCE, pp. 470–482.